ACS APPLIED MATERIALS & INTERFACES

Research Article

www.acsami.org

Controlling Effective Aspect Ratio and Packing of Clay with pH for Improved Gas Barrier in Nanobrick Wall Thin Films

David A. Hagen, Lauren Saucier, and Jaime C. Grunlan*

Department of Mechanical Engineering, Texas A&M University, College Station, Texas 77843, United States

Supporting Information

ABSTRACT: Polymer–clay thin films constructed via layer-by-layer (LbL) assembly, with a nanobrick wall structure (i.e., clay nanoplatelets as bricks surrounded by a polyelectrolyte mortar), are known to exhibit a high oxygen barrier. Further barrier improvement can be achieved by lowering the pH of the clay suspension in the polyethylenimine (PEI) and montmorillonite (MMT) system. In this case, the charge of the deposited PEI layer is increased in the clay suspension environment, which causes more clay to be deposited. At pH 4, MMT platelets deposit with near perfect ordering, observed with transmission electron microscopy, enabling a 5× improvement in the gas barrier for a 10 PEI/MMT bilayer thin film (85 nm) relative to the same film made with pH 10 MMT. This improved gas barrier approaches that achieved with much higher aspect ratio vermiculite clay. In essence, lower pH is generating a higher effective aspect ratio for MMT due to greater induced surface charge in the PEI layers, which causes heavier clay deposition. These flexible, transparent nanocoatings have a wide range of possible applications, from food and electronics packaging to pressurized bladders.

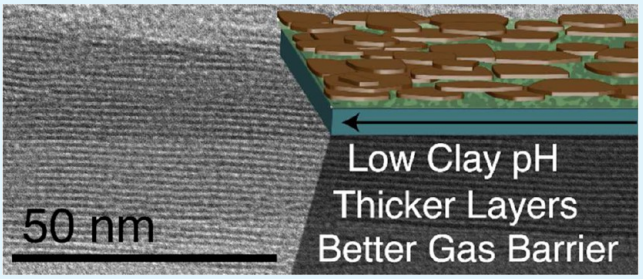

KEYWORDS: *layer-by-layer assembly, polyelectrolyte multilayer, oxygen barrier, transmission electron microscopy, clay, nanocoatings*

INTRODUCTION

Layer-by-layer (LbL) deposition is a simple, cost-effective, and versatile processing technique used to create functional thin film composites with exceptional properties on almost any substrate.[1,2] Thin films have been created that passively block gas[3] and heat,[4] respond to light,[5] heat,[6] and pH[7] (in various ways), conduct electricity,[8] and release medicinal molecules.[9] LbL assembly involves depositing species with complementary functionality, with electrostatic interaction being the most extensively studied driving force.[2] Various nanoparticles (with inherent or imparted functionalities) such as dots,[10] rods,[11] tubes,[12] sheets,[8] platelets,[13] and spheres[14] can be utilized to create highly organized structures one nanolayer at a time. Repeating sequences of three or more can be used if reinforcement of a previous layer or multiple component functionalities are employed.[15,16] Beyond materials used, there are many parameters that can be altered during deposition to further tailor the final thin film morphology (concentration, pH, solution temperature, ionic strength, charge density, molecular weight, and polymer chain architecture).[1,2] In the LbL literature, many studies have examined the influence of polyelectrolyte solution pH on the resultant thin film growth rate and morphology.[17−20] In addition to changing the charge density and resultant configuration of the polymer in an aqueous solution, altering one solution pH will also affect the charge density of the exposed polymer chains of the previously deposited layer.[21−23]

The present study shows that altering pH of the aqueous clay suspension changes the amount of clay deposited in the nanobrick wall structure (i.e., clay nanoplatelet bricks and polymer mortar). In the case of montmorillonite (MMT) clay platelets, charge density does not dramatically change with regard to suspension pH, but altering the pH of the clay alters the previously deposited polyethylenimine (PEI) layer. PEI is very highly charged at low pH and has only a low charge density at high pH.[24] Thicker polymer layers are deposited at pH 10 because PEI assumes a coiled conformation due to minimal self-repulsion in its low charge state.[20] MMT generates a basic pH (~10) in water, but adjusting it to a lower pH causes the previously deposited PEI to become highly charged, driving more clay to be deposited. An increase in the thickness of PEI/MMT bilayers (BL), as the MMT suspension pH is reduced, is shown schematically in Figure 1a. More clay in each deposited layer leads to an exceptional oxygen barrier, and these nanobrick wall structures (MMT bricks with PEI mortar) also exhibit flexibility and high transparency, which are desirable in barrier applications for food packaging, flexible electronics, and pressurized bladders.[25−27] Traditional barrier layers, such as metallized plastic or inorganic oxides (e.g., SiO_x), require complex processing and are prone to cracking and pinholes.[28,29] The polymer–clay nanocomposite thin films explored here are capable of reducing the amount of material used, while providing a more aesthetic (transparent) film, using a lower energy and environmentally friendly process.

Received: October 31, 2014
Accepted: December 4, 2014
Published: December 4, 2014

 © 2014 American Chemical Society

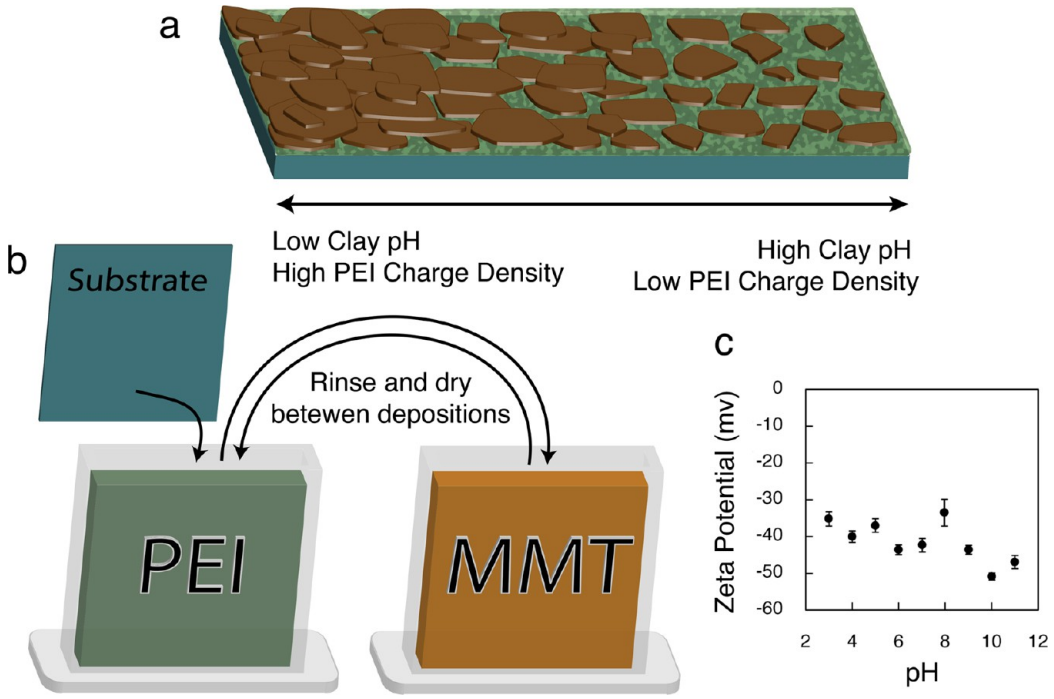

Figure 1. (a) Illustration of clay deposition onto PEI surface as a function of clay suspension pH, (b) schematic of layer-by-layer deposition process, and (c) ζ-potential of MMT clay as a function of pH.

EXPERIMENTAL SECTION

Materials. Branched polyethylenimine (M_w = 25 000 g/mol, ρ = 1.10 g/cm^3) was purchased from Sigma-Aldrich (St. Louis, MO) and used as a 0.1 wt % deionized (DI) water solution. Natural sodium montmorillonite clay (trade name Cloisite NA+), provided by Southern Clay Products, Inc. (Gonzales, TX), was dispersed as a 1 wt % suspension in deionized (DI) water by rolling in bottles overnight. MMT platelets have a reported density of 2.86 g/cm^3, diameter ranging from 10 to 1000 nm, and thickness of 1 nm.[30] The ζ-potential of MMT suspensions was measured with a ζ-phase angle light scattering (ZETA PALS) instrument (Brookhaven Instruments Corporation, Holtsville, NY).

Substrates. Poly(ethylene terephthalate) (PET) film, with a thickness of 179 μm (trade name ST505, produced by DuPont-Teijin), was purchased from Tekra (New Berlin, WI) and used as the substrate for oxygen transmission rate (OTR) testing and transmission electron microscopy (TEM). This PET film has an OTR of approximately 8.6 cm^3/(m^2·day·atm) under dry conditions.[20] Prior to deposition, PET substrates were rinsed with methanol and DI water, followed by treatment of each side of the substrate using a BD-20C Corona Treater (Electro-Technic Products, Inc., Chicago, IL) to ensure an adequate negative surface charge before coating. Polished silicon wafers, purchased from University Wafer (South Boston, MA), were used as substrates for profilometry and atomic force microscopy (AFM). Silicon wafers were rinsed with acetone and DI water and then plasma treated for 5 min immediately before use. Thin films to be used for thermogravimetric analysis (TGA) were deposited onto polytetrafluoroethylene (PTFE) sheets purchased from McMaster-Carr (Elmhurst, IL). The PTFE sheets were rinsed with ethanol and water, but corona treatment was omitted to cause weaker adhesion and ultimately produce freestanding films.

Layer-by-Layer Assembly Procedure. All deposition was carried out at room temperature by an automated dipping system.[31] Each substrate was dipped into the cationic 0.1 wt % PEI solution (adjusted to pH 10.0 using 1 M HCl) for 1 min. After this, and every subsequent dip, the substrate was rinsed with DI water and dried with filtered air. The substrate was then dipped into a 1 wt % anionic MMT clay suspension for 1 min (adjusted using 1 M HCl), which completed a single bilayer (BL) dipping cycle, as illustrated in Figure 1b. This process was repeated until x bilayers were obtained, denoted as $[PEI_{10}/MMT_y]_x$, where y is the MMT suspension pH. After the final rinsing and air drying, the films deposited onto PET were dried in an oven at 70 °C for 15 min.

Thin Film Characterization. Film thickness was measured as a function of bilayers deposited with a P6 profilometer (KLA-Tencor, Milpitas, CA). Multiple scratches were made through each film so that height from the leveled substrate could be measured, and each data point reported is an average of values from three wafers. Mass deposition onto Ti/Au plated quartz crystals was measured using a research quartz crystal microbalance (QCM) (Maxtek Inc., Cypress, CA) by measuring the resonant frequency value of the crystal after every drying step. Atomic force microscopy (AFM) was performed with a Dimension Icon AFM (Bruker, Billerica, MA) in tapping mode with an HQ:NSC35/Al BS probe (Mikromasch, Lady's Island, SC). Root-mean-square roughness (R_q) measurements were taken from a 20 × 20 μm area. TGA was performed with a Q50 thermogravimetric analyzer (TA Instruments, New Castle, DE). 200 BL films on PTFE substrates were soaked in DI water overnight and scraped off using a razor blade in a sweeping motion to ensure the substrate was not scraped off with the film. The film was heated at 10 °C/min to 120 °C and held for 1 h to remove all excess moisture. The film was then heated at the same rate to 650 °C and held for 1 h. Clay concentration was calculated as the mass remaining at the end of the test divided by the mass at the end of the 120 °C holding period. OTR testing was performed according to ASTM D-3985 specifications by MOCON (Minneapolis, MN) using an Oxtran 2/21 ML instrument at 23 °C and 0% RH. Samples for TEM were prepared by embedding the film in Epofix resin (EMS, Hatfield, PA) overnight and cutting sections, using an Ultra 45° diamond knife (Diatome, Hatfield, PA) at a 6° angle, onto 300 mesh copper grids. TEM micrographs of the thin film cross sections (~90 nm thick) were imaged using a Tecnai G2 F20 (FEI, Hillsboro, OR) at an accelerating voltage of 200 kV.

RESULTS AND DISCUSSION

Influence of pH on Film Growth. Using two polymers that have inherently low charge densities in their own solution, but become highly charged when exposed to the pH condition of the other solution, allows for very thick multilayer growth.[21]

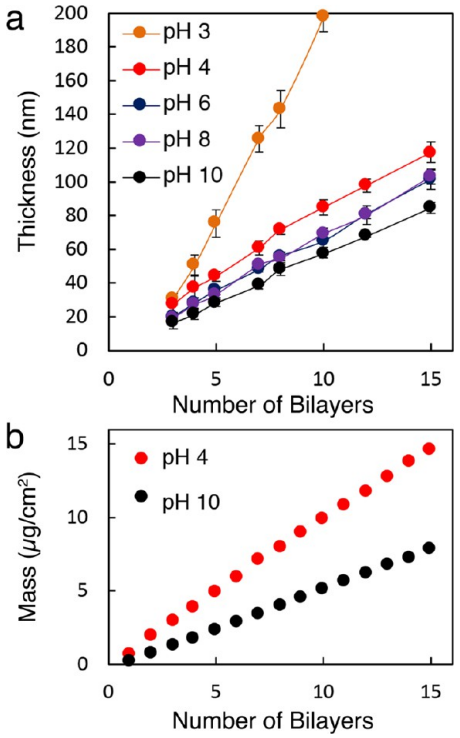

Figure 2. (a) Thickness of pH 10 PEI deposited with MMT of varying pH. The lines shown are simply a guide for the eye. (b) Mass deposition of PEI_{10}/MMT_x at clay pH of 4 and 10.

The high surface charge of the previously deposited polymer layer causes a thick deposition of the following layer in order to satisfy this imparted charge. This technique has primarily been used for weak polyelectrolytes,[2] but the same concept can be used to increase the growth rate of a polymer/nanoparticle system.[22] In the present study, PEI at pH 10 is combined with MMT at varying pH. Figure 1c shows that the ζ-potential of MMT platelets in aqueous suspension is not highly dependent upon pH, fluctuating between −30 and −50 mV in the pH range of 3−11, which is due to the dominating permanent negative charge of the MMT platelet basal planes (as a result of isomorphic substitutions).[32] The amphoteric edge sites are positively charged below and negatively charged above pH 6.5, but have only a small influence on ζ-potential.[32] In contrast, polyethylenimine charge density is highly dependent upon pH.[24] At pH 10, there is less than 5% protonation, but many of the amine groups become protonated as the pH decreases (approximately 60% protonation at pH 4).[24]

In an effort to deposit more MMT platelets in a given deposition cycle, the pH of the clay suspension was reduced, which dramatically increased the charge density of the previously deposited PEI layer. This increase in charge density attracts more clay platelets to the surface, creating a thicker, more densely packed layer, shown schematically in Figure 1a. The $PEI_x/MMT_{9.7}$ (the unaltered MMT suspension is pH 9.7) system was previously studied to examine the influence of PEI pH on film growth.[20] The thickest growth was achieved at pH 10, with a linear growth rate of approximately 3 nm/BL through 20 BL. The growth of PEI_{10}/MMT_x is shown in Figure 2a to be significantly greater as the pH of the MMT suspension decreases, due to an increased amount of MMT deposited.

QCM reveals a significant increase in mass deposited for the lower pH clay system, shown in Figure 2b. Clay concentration

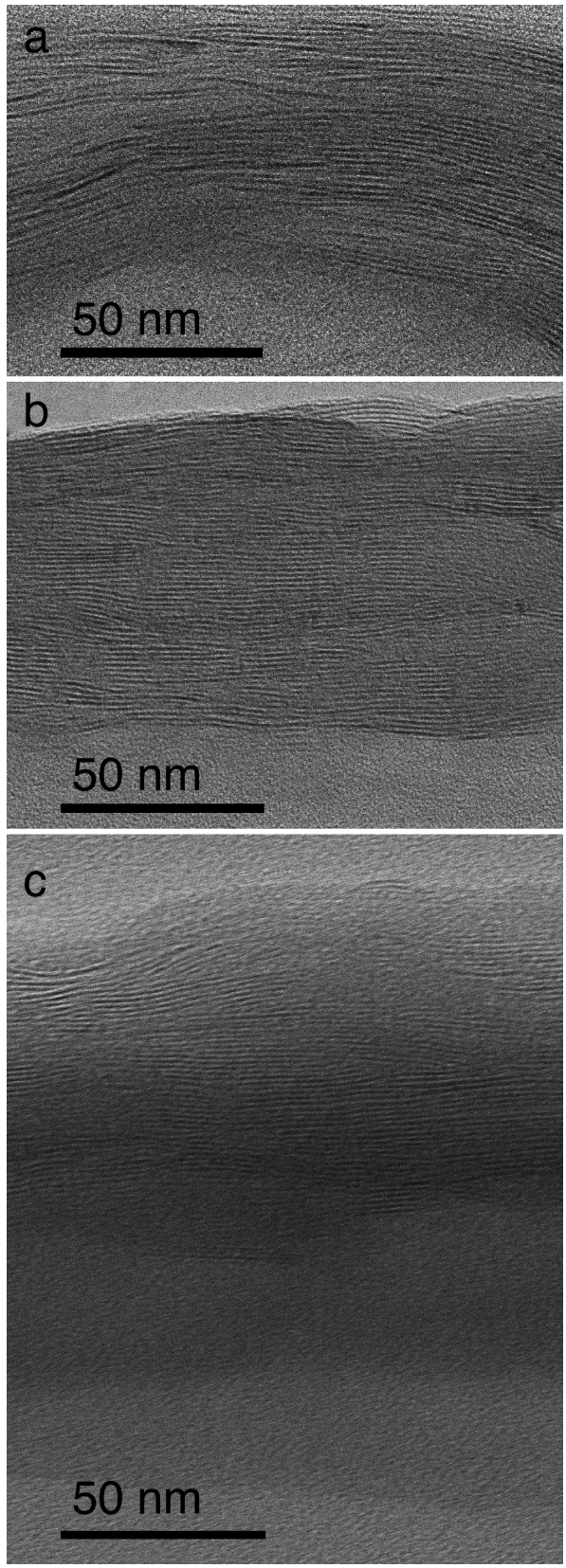

Figure 3. TEM micrographs of 10 BL (a) PEI_{10}/MMT_{10}, (b) PEI_{10}/MMT_4, and (c) PEI_{10}/MMT_3 deposited on PET film.

of the film could not be calculated using QCM due to instances where the total mass was reduced after the PEI deposition, from desorption of some of the outermost clay platelets (and

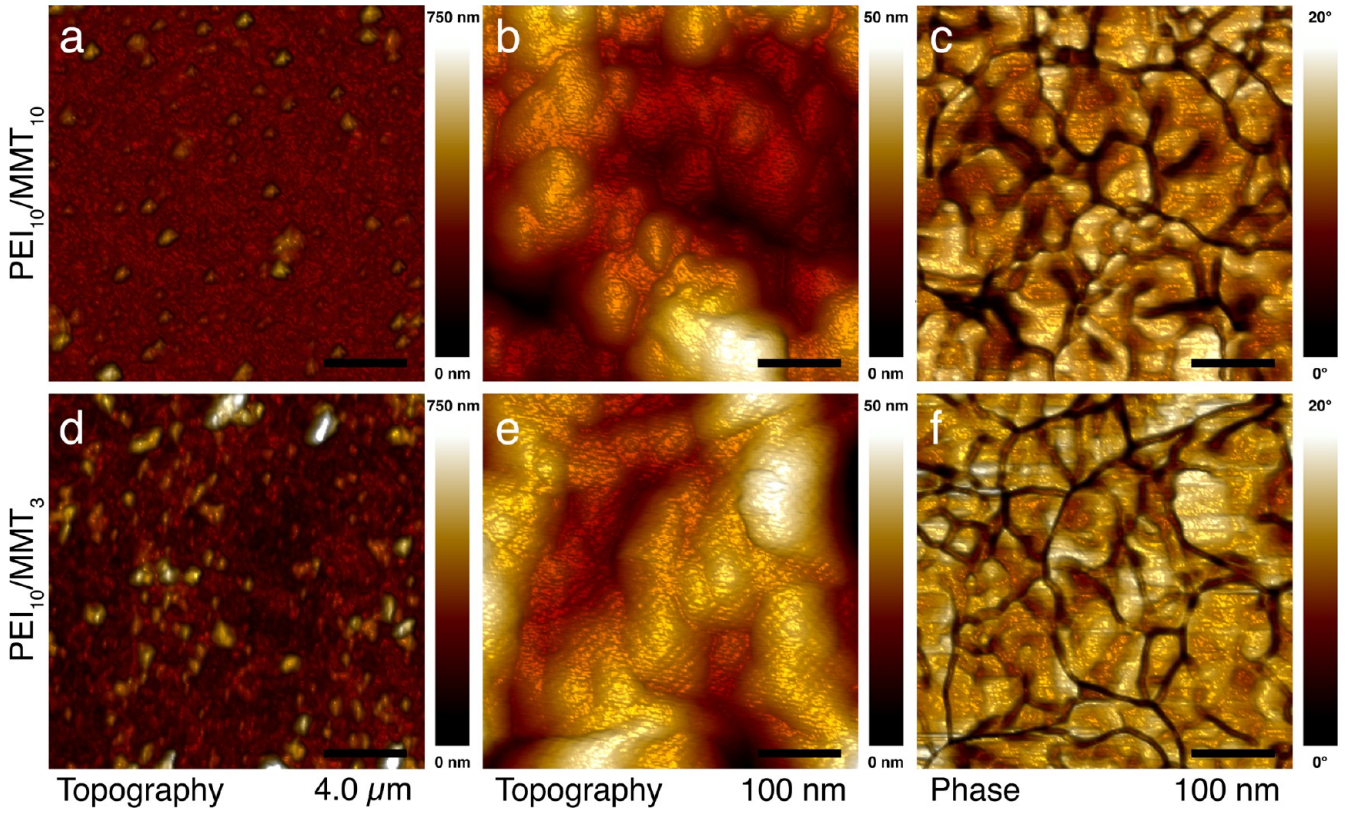

Figure 4. AFM topography (a,b,d,e) and phase images (c,f) of $[PEI_{10}/MMT_{10}]_{15}$ (top-a,b,c) and $[PEI_{10}/MMT_3]_{15}$ (bottom-d,e,f). The phase images highlight the cobblestone path structure of the MMT-covered surface and correspond to the adjacent topography (i.e., height) images (b,e).

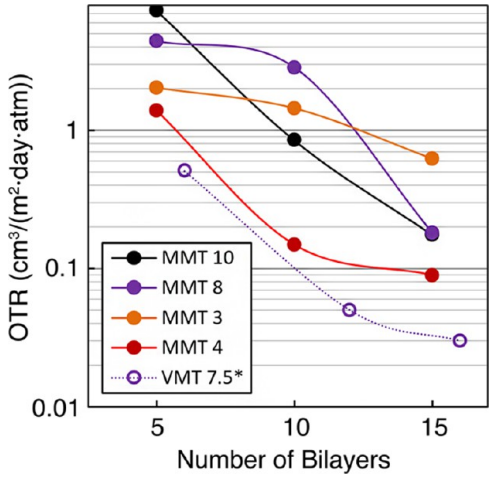

Figure 5. Oxygen transmission rate as a function of $PEI_{10}/clay_y$ bilayers deposited at varying pH (y denotes MMT suspension pH). Lines are only meant as a guide. The data set with open circles represents PEI deposited with vermiculite clay from ref 36.

replacement by PEI of less mass). Clay concentration was instead calculated using TGA to be 77 wt % for PEI_{10}/MMT_{10} and 80 wt % for PEI_{10}/MMT_4. These values are extremely high relative to conventional clay-filled composites.[33] There is an increase in concentration due to additional clay being added every deposition step as the pH of the clay solution is reduced due to the PEI-covered surface being highly charged. This difference is somewhat diminished by additional PEI being deposited for the lower pH system. In an effort to demonstrate the full extent of this pH change on clay deposition, the amount of clay added per bilayer was calculated to increase from 0.42 to 0.79 $\mu g/cm^2$, almost doubling the amount of clay added per bilayer simply by lowering the pH of the clay solution. This was calculated by multiplying the average mass per bilayer obtained with the QCM by the clay mass fraction from TGA.

This high level of clay loading for the various films can be seen in TEM cross-sectional images, shown in Figure 3. For MMT at pH 10 (Figure 3a), there are areas of highly ordered clay platelets and also areas with gaps in the clay. In contrast, the PEI_{10}/MMT_4 film (Figure 3b) shows a very well-ordered structure in the majority of the thin film. The PEI_{10}/MMT_3 film is also well-ordered (Figure 3c), but there are areas of misalignment within the tightly packed structure, potentially from a small amount of edge-to-face bonding among the MMT platelets. This interaction occurs readily with indifferent electrolytes (such as NaCl) in solution below pH 6.5 (below this pH, the edges are positively charged).[32] The indifferent electrolytes promote edge-to-face bonding by shielding opposing basal charges, but it is conceivable that some edge-to-face bonding may occur in the highly confined packing of this film. At pH 3, the clay platelet edges have a higher positive charge and can be attracted to the negatively charged face of the deposited MMT. The AFM surface roughness values (R_q) are similar for clay pH values of 4, 8, and 10 (~30 nm), but roughness triples (to 85 nm) for PEI_{10}/MMT_3, agreeing with the waviness observed in TEM micrographs (Figure 3c). AFM topography of the pH 10 (Figure 4a,b) and pH 3 (Figure 4d,e) films shows the lower pH film to be much rougher at a scan size of 20 μm, but at a smaller scan size of 500 nm, the features are similar, and the surfaces appears smooth without visible platelet edges. The phase images highlight the cobblestone path structure of the top layer, with many platelets visible in the

100−200 nm range (Figure 4c,f). Uninterrupted platelets as large as 800 nm were observed in the pH 3 system using a larger scan size (see the Supporting Information). These larger platelets may have been a factor in creating a rougher film.

Oxygen Permeability of Thin Films. Figure 5 shows oxygen transmission rate as a function of PEI_{10}/MMT_x bilayers deposited. For PEI_{10}/MMT_8, there is no improvement over PEI_{10}/MMT_{10} beyond 5 BL. At pH 4, there is more than a 5× improvement in OTR relative to the film prepared with pH 10 at 5 and 10 BL. The effective permeability (calculated using a previously described method)[34] of the $[PEI_{10}/MMT_4]_{10}$ film is 2.9×10^{-20}·cm^3·cm/(cm^2·s·Pa), which is less than half the permeability reported for vapor deposited SiO_x coatings.[35] $[PEI_{10}/MMT_4]_{15}$ has an OTR of 0.09 cm^3/(m^2·day·atm) that is 2 orders of magnitude lower than that of the bare PET substrate that is 3 orders of magnitude thicker. This level of oxygen barrier approaches that of PEI/vermiculite (VMT) bilayers reported previously.[36] VMT is a clay platelet that has an aspect ratio approximately 1 order of magnitude larger than that of MMT. Larger aspect ratio clay creates a more tortuous pathway for gas molecules through the film, creating a lower transmission rate. By reducing the pH of the MMT solution, deposited layers behave as though there is a much greater effective aspect ratio (similar to skewed stacks observed in composites exposed to shear stress).[37] The pH 3 system shows improved performance at 5 BL, but is a poorer barrier than PEI_{10}/MMT_{10} at 10 and 15 BL. This is probably due to the large amount of material deposited quickly at low clay pH, but the reduced order diminishes the effectiveness of the tortuous path at 10 and 15 BL. Alignment of the clay platelets is crucial for high barrier films because they cause oxygen molecules to spend more time traveling laterally through the film rather than through the thickness.

CONCLUSION

Polymer nanocomposite thin film oxygen barriers were deposited with the LbL process as a foil or SiO*x* replacement. Depositing polyethylenimine from pH 10 solution and montmorillonite clay from varying pH suspensions, it was shown that the density of clay layers, and ultimately gas barrier, was altered. By reducing the pH of the clay suspension, the PEI surface became highly charged, producing a greater, more ordered deposition of MMT clay platelets. A 10 BL film deposited with pH 4 MMT provided a 5× improvement in oxygen transmission rate over the same film prepared with pH 10 clay and 2 orders of magnitude improvement over the 179 μm PET substrate. This pH 4 performance is comparable to that of a similar number of bilayers prepared with vermiculite clay,[35] which has an aspect ratio approximately 10× greater. At pH < 4, higher positive charge on the clay platelet edges leads to some disorder in clay orientation, and the barrier is degraded. This ability to increase the effective clay aspect ratio with pH provides a means to achieve high gas barrier with lower-cost, easier-to-process clays. These water-based nanocoatings could be used to improve the performance of plastic film used for food, pharmaceutical, and electronics packaging.

ASSOCIATED CONTENT

Supporting Information

Additional AFM topography and corresponding phase images of $[PEI_{10}/MMT_y]_{15}$. This material is available free of charge via the Internet at http://pubs.acs.org.

AUTHOR INFORMATION

Corresponding Author

*J. C. Grunlan. E-Mail: jgrunlan@tamu.edu.

Notes

The authors declare no competing financial interest.

ACKNOWLEDGMENTS

The authors acknowledge the Texas A&M Engineering Experiment Station for infrastructural support of this work.

REFERENCES

(1) Decher, G.; Schlenoff, J. B. *Multilayer Thin Films*; Wiley-VCH Verlag GmbH & Co. KGaA: Weinheim, Germany, 2012.

(2) Borges, J.; Mano, J. F. Molecular Interactions Driving the Layer-by-Layer Assembly of Multilayers. *Chem. Rev.* **2014**, *114*, 8883−8942.

(3) Hagen, D. A.; Foster, B.; Stevens, B.; Grunlan, J. C. Shift-Time Polyelectrolyte Multilayer Assembly: Fast Film Growth and High Gas Barrier with Fewer Layers by Adjusting Deposition Time. *ACS Macro Lett.* **2014**, 663−666.

(4) Cain, A. A.; Plummer, M. G.; Murray, S. E.; Bolling, L.; Regev, O.; Grunlan, J. Iron-Containing, High Aspect Ratio Clay as Nanoarmor That Imparts Substantial Thermal/Flame Protection to Polyurethane with a Single Electrostatically-Deposited Bilayer. *J. Mater. Chem. A* **2014**, *2*, 17609−17617.

(5) Borges, J.; Rodrigues, L. C.; Reis, R. L.; Mano, J. F. Layer-by-Layer Assembly of Light-Responsive Polymeric Multilayer Systems. *Adv. Funct. Mater.* **2014**, *24*, 5624−5648.

(6) Zhou, J.; Pishko, M. V.; Lutkenhaus, J. L. Thermoresponsive Layer-by-Layer Assemblies for Nanoparticle-based Drug Delivery. *Langmuir* **2014**, *30*, 5903−5910.

(7) Quadir, M. A.; Morton, S. W.; Deng, Z. J.; Shopsowitz, K. E.; Murphy, R. P.; Epps, T. H.; Hammond, P. T. PEG−Polypeptide Block Copolymers as pH-Responsive Endosome-Solubilizing Drug Nanocarriers. *Mol. Pharmaceutics* **2014**, *11*, 2420−2430.

(8) Stevens, B.; Dessiatova, E.; Hagen, D. A.; Todd, A. D.; Bielawski, C. W.; Grunlan, J. C. Low-Temperature Thermal Reduction of Graphene Oxide Nanobrick Walls: Unique Combination of High Gas Barrier and Low Resistivity in Fully Organic Polyelectrolyte Multilayer Thin Films. *ACS Appl. Mater. Interfaces* **2014**, *6*, 9942−9945.

(9) Ariga, K.; Kawakami, K.; Ebara, M.; Kotsuchibashi, Y.; Ji, Q.; Hill, J. P. Bioinspired Nanoarchitectonics as Emerging Drug Delivery Systems. *New J. Chem.* **2014**, *38*, 5149−5163.

(10) Xiao, F. X.; Miao, J. W.; Liu, B. Layer-by-Layer Self-Assembly of CdS Quantum Dots/Graphene Nanosheets Hybrid Films for Photoelectrochemical and Photocatalytic Applications. *J. Am. Chem. Soc.* **2014**, *136*, 1559−1569.

(11) Placido, T.; Fanizza, E.; Cosma, P.; Striccoli, M.; Curri, M. L.; Comparelli, R.; Agostiano, A. Electroactive Layer-by-Layer Plasmonic Architectures Based on Au Nanorods. *Langmuir* **2014**, *30*, 2608−2618.

(12) Saetia, K.; Schnorr, J. M.; Mannarino, M. M.; Kim, S. Y.; Rutledge, G. C.; Swager, T. M.; Hammond, P. T. Spray-Layer-by-Layer Carbon Nanotube/Electrospun Fiber Electrodes for Flexible Chemiresistive Sensor Applications. *Adv. Funct. Mater.* **2014**, *24*, 492−502.

(13) Meaud, J.; Sain, T.; Yeom, B.; Park, S. J.; Shoultz, A. B.; Hulbert, G.; Ma, Z.-D.; Kotov, N. A.; Hart, A. J.; Arruda, E. M.; Waas, A. M. Simultaneously High Stiffness and Damping in Nanoengineered Microtruss Composites. *ACS Nano* **2014**, *8*, 3468−3475.

(14) Yanagida, S.; Kosakai, Y.; Yasumori, A. Preparation of Gold Nanoparticle Dispersed TiO_2-Polymer Composite Film by a Combined Layer-by-Layer and Photocatalytic Deposition Method. *Colloids Surf., A* **2014**, *456*, 55−61.

(15) Hagen, D. A.; Box, C.; Greenlee, S.; Xiang, F.; Regev, O.; Grunlan, J. C. High Gas Barrier Imparted by Similarly Charged Multilayers in Nanobrick Wall Thin Films. *RSC Adv.* **2014**, *4*, 18354−18359.

(16) Lutkenhaus, J. L.; Olivetti, E. A.; Verploegen, E. A.; Cord, B. M.; Sadoway, D. R.; Hammond, P. T. Anisotropic Structure and Transport

in Self-Assembled Layered Polymer−Clay Nanocomposites. *Langmuir* **2007**, *23*, 8515−8521.
(17) Shiratori, S. S.; Rubner, M. F. pH-Dependent Thickness Behavior of Sequentially Adsorbed Layers of Weak Polyelectrolytes. *Macromolecules* **2000**, *33*, 4213−4219.
(18) Bieker, P.; Schönhoff, M. Linear and Exponential Growth Regimes of Multilayers of Weak Polyelectrolytes in Dependence on pH. *Macromolecules* **2010**, *43*, 5052−5059.
(19) Yoo, D.; Shiratori, S. S.; Rubner, M. F. Controlling Bilayer Composition and Surface Wettability of Sequentially Adsorbed Multilayers of Weak Polyelectrolytes. *Macromolecules* **1998**, *31*, 4309−4318.
(20) Priolo, M. A.; Gamboa, D.; Grunlan, J. C. Transparent Clay−Polymer Nano Brick Wall Assemblies with Tailorable Oxygen Barrier. *ACS Appl. Mater. Interfaces* **2010**, *2*, 312−320.
(21) Yang, Y.-H.; Haile, M.; Park, Y. T.; Malek, F. A.; Grunlan, J. C. Super Gas Barrier of All-Polymer Multilayer Thin Films. *Macromolecules* **2011**, *44*, 1450−1459.
(22) Peng, C.; Thio, Y. S.; Gerhardt, R. A.; Ambaye, H.; Lauter, V. pH-Promoted Exponential Layer-by-Layer Assembly of Bicomponent Polyelectrolyte/Nanoparticle Multilayers. *Chem. Mater.* **2011**, *23*, 4548−4556.
(23) Choi, J.; Rubner, M. F. Influence of the Degree of Ionization on Weak Polyelectrolyte Multilayer Assembly. *Macromolecules* **2004**, *38*, 116−124.
(24) Mészáros, R.; Thompson, L.; Bos, M.; de Groot, P. Adsorption and Electrokinetic Properties of Polyethylenimine on Silica Surfaces. *Langmuir* **2002**, *18*, 6164−6169.
(25) Graff, G. L.; Burrows, P. E.; Williford, R. E.; Praino, R. F. Barrier Layer Technology for Flexible Displays. In *Flexible Flat Panel Displays*; Crawford, G. C., Ed.; John Wiley & Sons, Ltd: Chichester, U. K., 2005; pp 57−77.
(26) Bowles, M.; Jianjun, L. Review on Nanotechnology in Agricultural Products Logistics Management. In *8th International Conference on Computing and Networking Technology (ICCNT)*, Gyeongju, Korea, August 27−29, 2012; IEEE: New York, 2012; pp 415−420.
(27) Yam, K. L.; Lee, D. S. *Emerging Food Packaging Technologies: Principles and Practice*; Woodhead Publishing: Cambridge, U. K., 2012.
(28) Leterrier, Y. Durability of Nanosized Oxygen-Barrier Coatings on Polymers. *Prog. Mater. Sci.* **2003**, *48*, 1−55.
(29) Affinito, J. D.; Gross, M. E.; Coronado, C. A.; Graff, G. L.; Greenwell, E. N.; Martin, P. M. A New Method for Fabricating Transparent Barrier Layers. *Thin Solid Films* **1996**, *290*, 63−67.
(30) Ploehn, H. J.; Liu, C. Y. Quantitative Analysis of Montmorillonite Platelet Size by Atomic Force Microscopy. *Ind. Eng. Chem. Res.* **2006**, *45*, 7025−7034.
(31) Jang, W.-S.; Grunlan, J. C. Robotic Dipping System for Layer-by-Layer Assembly of Multifunctional Thin Films. *Rev. Sci. Instrum.* **2005**, *76*.
(32) Tombácz, E.; Szekeres, M. Colloidal Behavior of Aqueous Montmorillonite Suspensions: The Specific Role of pH in the Presence of Indifferent Electrolytes. *Appl. Clay Sci.* **2004**, *27*, 75−94.
(33) Podsiadlo, P.; Kaushik, A. K.; Arruda, E. M.; Waas, A. M.; Shim, B. S.; Xu, J. D.; Nandivada, H.; Pumplin, B. G.; Lahann, J.; Ramamoorthy, A.; Kotov, N. A. Ultrastrong and Stiff Layered Polymer Nanocomposites. *Science* **2007**, *318*, 80−83.
(34) Nielsen, L. E. Models for the Permeability of Filled Polymer Systems. *J. Macromol. Sci., Pure Appl. Chem.* **1967**, *1*, 929−942.
(35) Roberts, A.; Henry, B.; Sutton, A.; Grovenor, C.; Briggs, G.; Miyamoto, T.; Kano, M.; Tsukahara, Y.; Yanaka, M. Gas Permeation in Silicon-Oxide/Polymer (Siox/Pet) Barrier Films: Role of the Oxide Lattice, Nano-Defects and Macro-Defects. *J. Membr. Sci.* **2002**, *208*, 75−88.
(36) Priolo, M. A.; Holder, K. M.; Greenlee, S. M.; Grunlan, J. C. Transparency, Gas Barrier, and Moisture Resistance of Large-Aspect-Ratio Vermiculite Nanobrick Wall Thin Films. *ACS Appl. Mater. Interfaces* **2012**, *4*, 5529−5533.
(37) Fornes, T. D.; Yoon, P. J.; Keskkula, H.; Paul, D. R. Nylon 6 Nanocomposites: The Effect of Matrix Molecular Weight. *Polymer* **2001**, *42*, 09929−09940.